PHYSICAL PROCESSES GOVERNING ELECTRIC CURRENTS IN A HALL THRUSTER

R. Santos * **and E. Ahedo** †

E.T.S. Ingenieros Aeronáuticos, Universidad Politécnica de Madrid, Madrid, Spain

ABSTRACT

The discharge current and the ion current in the plume of a Hall thruster are generally known from experiments. The difference between these two currents is the axial upstream electron current. This work discusses the physical processes that determine the ion and electron currents, paying special attention on the role of secondary electron emission and plasma-wall interaction. Using an upgraded version of the hybrid HPHall-2 code, we show the relevance of the Bohm-type turbulence on the electron perpendicular transport, and we remark the influence of the numerical models of the plasma-production and the plasma-wall interaction on the performace of the thruster. We also estimate the ionization produced by the free secondary electron beams within the plasma.

1. INTRODUCTION

An operational point of a conventional Hall thruster is characterized generally by the discharge voltage, the mass flow of injected gas, and the current through the magnetic circuit that sets the magnetic strength in the discharge channel. The two main output magnitudes are the discharge current I_d and the current of the ion beam. The discharge current is the electron current emitted by the neutralizing cathode placed in the near plume. This electron current splits in an outgoing fraction that neutralizes the ion beam and an inward current that is responsible of the ionization of the injected neutral gas. Thus, the plasma discharge between the anode and the virtual neutralization surface is characterized by the outwards ion and inwards electron currents there, I_{iP} and $I_{eP} = I_d - I_{iP}$, respectively.

The inwards electron current is channeled azimuthally by the combination of the mainly-radial magnetic field and the axial electric field. The transport of the electron flow perpendicular to the magnetic field (i.e. B-perpendicular) is very limited and caused by collisional effects. The ratio of axial-to-azimuthal electron currents is equal to the Hall parameter or ratio between total collision frequency and electron gyrofrequency. The diffusive axial electron motion at the exit of the chamber is characterized by an Ohm's law stating that the axial electron is equal to the B-perpendicular conductivity times the electric field. Early measurements at the dawn of the research in het, already found that the classical diffusion, based on electron-neutral and electron-ion collisions, was too small to justify the large electron current. Either turbulent diffusion or wall-interaction phenomena were postulated as probable mechanisms for that anomalous diffusion [1]. Since then, the innumerable experiments on het discharges confirm that anomalous diffusion seems to exist.

Both turbulent diffusion and wall diffusion are included customarily in fluid and particle models of the het discharge. Advances in the understanding on the wall-interaction phenomena have permitted to model approximately anomalous diffusion caused by plasma-wall interaction, in terms of other plasma magnitudes [2]. Implementing that wall-interaction model in fluid and hybrid codes, Ahedo and coworkers [3, 4] found that wall collisionality by itself is not able to provide the anomalous diffusion suggested by experiments, leaving turbulent diffusion as the main candidate for the anomalous behavior. Later, Garrigues et al. [5] reached the same conclusion.

There does not exist yet any satisfactory theory explaining and modeling turbulent diffusion. There is the vague idea that turbulent diffusion is due to the correlation of low-frequency azimuthal perturbations of plasma density and electric potential [6], although other authors claim it to be caused by high-frequency oscillations of the plasma [7]. Hence, full models of the plasma discharge include turbulent diffusion as an extra phenomenological term on the total collisional frequency. This term is proportional to the electron gyrofrequency, as in Bohm-type diffusion [8]. The models just tune the Bohm coefficient in order to match the total collision frequency (in fact, the discharge current) to experimental values. In most HET models, the Bohm coefficient seems to be several times smaller than 1/16.

*PhD Candidate, robert.santos@upm.es

†Professor, eduardo.ahedo@upm.es

Recently, some authors have treated the Bohm coefficient as variable along the chamber and have adjusted this Bohm parameter function in order to fit better the plasma axial profiles. The interest of this ad hoc adjustment would merely be to identify whether the turbulent diffusion is concentrated in one region of the discharge. Unfortunately, there is no agreement among authors, who are divided into placing turbulent diffusion preferentially inside the chamber [9], outside the chamber [10, 11], or out of the maximum electric field region [12, 13].

Katz and coworkers [14], working with the hybrid simulation code HPHall-2 [4] and trying to simulate the SPT-100 thruster [15], point out that the estimate of the ion current is too low and discuss possible ways of ion current enhancement. First they note that the ionization cross-section data for double ions used by the code is much underestimated and implement a better data. Second, they propose ion reflux in the plume as an enhancement mechanism. As a result of these changes, I_{iP} increases. Then, in order to keep I_d constant, I_{eP} must decrease, which is achieved by decreasing the Bohm coefficient. The results they get lead them to conclude that the need to invoke turbulent diffusion as a relevant mechanism in the HET discharge is highly reduced. This conclusion seems clearly at odds with experimental evidence and suggests that somehow the implemented changes are overestimating the ion current.

The reality is that ion and electron currents are affected by a variety of physical mechanisms, generally in a complex way. In addition, the reliability or accuracy of the modelling of these mechanisms is not good enough in all cases. This paper attempts to discuss the influence of those mechanisms and the way they are modelled. The hybrid code used here for the simulations is an evolution of HPHall-2. The main improvements are reported in Refs. [16, 17, 18].

The layout of the paper is the following. In section 2 we discuss the physical processes concerning the ion and the electron currents. In section 3 we study the influence of the plasma-wall interaction on these currents, and the effect of secondary electrons in the plasma production is estimated in section 4. Finally, conclusions are presented in section 5.

2. BASIC EFFECTS

2.1. The ion beam current

The ion flow in a Hall thruster is almost collisionless and unmagnetized, thus ions are free accelerated by the ambipolar electric field. It is well known by the community that the structure of the ion flow consists of three regions [19]: the ion backstreaming region near the anode, the ionization region, and the acceleration region, which in general includes part of the channel and part of the plume.

The ion beam current is defined as the flux of ions through the plume of the thruster. This ion current is mainly determined by the mass flow and the discharge potential of the thruster. Studies about the influence of these operational parameters on the ion beam current, and hence on the performance of the thruster, can be found in many works [20, 21].

We focus on the physical processes that affect the ion beam current and the mechanisms to control it. The most important process is the ionization of neutrals by the primary electron population within the thruster. Although many models only take into account the simple ionization from the ground state, many studies point out the relevance of the multiply charged ions in the physics of the thruster.

Our hybrid code used in the simulations computes the simple and double ionization of the neutrals, which means three ionization events. First, the simple ionization of neutrals, which we compute taking the Drawin ionization model [22]. Second, the double ionization of neutrals, which is based on the experimental data of Mathur and Badrinathan [23], and is computed approximately according to the Drawin ionization formula [22]. And third, the ionization of simple ions, that is from Xe^{+} to Xe^{++}, which, following Katz et al.[14], is based on the work of Bell et al.[24], who provided experimental data and a fitting expression for the ionization rate. In all cases, the electrons are assumed Maxwellian.

The resulting ion production is:

$$\dot{n}_{i1} = n_n n_e \langle R_i \rangle_{0\to 1} \tag{1}$$

$$\dot{n}_{i2} = n_n n_e \langle R_i \rangle_{0\to 2} + n_{i1} n_e \langle R_i \rangle_{1\to 2} \tag{2}$$

where $\dot{n}_{i1}$ is the production of simple ions, $\dot{n}_{i2}$ is the production of double ions, n_n is the neutral density, n_e is the electron density, and $\langle R_i \rangle$ is the ionization rate of the different ionization events for Maxwellian electrons. Figure 1 shows the different ionization rates for a typical range of the electron temperature.

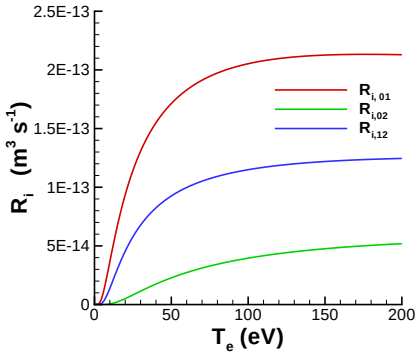

Figure 1. Ionization rates for Maxwellian electrons.

Another important process that governs the ion beam current is the plasma-wall interaction, where the ion outflow

imposed by the presence of the negative sheaths at walls, is recombined into a flux of neutrals coming back to the bulk region. The recombination at walls fulfills mass and flux conservation, and is responsible of a decay in the propellant utilization, because the new neutrals are affected by the wall accommodation process.

Hofer et al. [11] suggested the modification of the accommodation model based on the fraction of the neutrals affected by the accomodation rather than a change in the accommodation coefficient used. This new model increases the neutral density, and thus the ion production, in a similar way as the variation of the accommodation coefficient does. The effect on propellant utilization is not negligible. However there are scarce data on the matter, and we think that the suggested modification is not clear enough according to the physics of the plasma-wall interaction, thus we take the original wall accommodation model of [4].

The remaining collisional processes that affect the ion beam current are the bulk recombination and the charge exchange (CEX) collisions. The bulk recombination of ions is very small compared to the ionization, and can be neglected in the simulations. The CEX collisions may be important in the near-plume region of the thruster. However, in our simulation code this kind of collisions is not implemented yet, and its analysis remains for future work.

The charge conservation equation for the ions, once integrated in the whole simulation region and averaged in time, reads,

$$I_{i,b} = \mathcal{I}_{i,tot} - I_{i,a} - I_{i,w}, \tag{3}$$

where $I_{i,b}$ is the averaged ion beam current, $\mathcal{I}_{i,tot}$ is the averaged charge production along the total simulation time, $I_{i,a}$ is the averaged backstreaming ion current to the anode, and $I_{i,w}$ is the averaged ion current to the laterals walls of the thruster.

The $I_{i,a}$ current is small compared with $\mathcal{I}_{i,tot}$ and $I_{i,w}$. Thus to increase the $I_{i,b}$ current there are two mechanisms, a greater production, or smaller ion wall losses. The effect of these mechanisms is numerically studied, and the discussion of the results is presented in section 2.3.

2.2. The electron current

The electron current is the inwards electron flow from the cathode to the anode. Electrons are highly magnetized and effectively confined by the thruster lateral walls, with the thermalization frequency being much greater than the electron transit time in the channel. Thus a diffusive-fluid model for the perpendicular transport to the magnetic field is adopted, where the azimuthal $\mathbf{E} \times \mathbf{B}$ drift is recovered, and the small axial drift is determined by the classical collision frequency $\nu_c = \nu_{en} + \nu_{ei}$, with ν_{en} the electron-neutral collision frequency and ν_{ei} the electron-ion collision frequency. The typical magnetic field lines and the geometry of the SPT-100 Hall thruster are shown in figure 2.

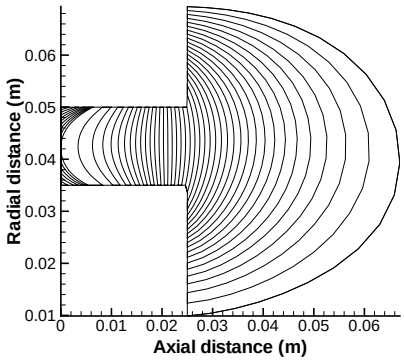

Figure 2. Magnetic field lines of the SPT-100 Hall thruster.

However, experimental data have shown that the classical collision frequency is insufficient to explain the high electron current measured inside the channel[1, 6]. To increase the axial drift velocity $\mathbf{u}_e$ of the electrons, an effective collision frequency ν_e is defined, which takes into account the plasma-wall interaction and the presence of turbulence within the plasma. The resulting momentum equation of the macroscopic-fluid model of the electrons across the B-field (axial direction) leads to the generalized Ohm law:

$$j_{e\perp} = \sigma_\perp \left(E_\perp + \frac{1}{en_e} \nabla_\perp (n_e T_e) \right), \tag{4}$$

with $\sigma_\perp = e^2 n_e \nu_e / (m_e \omega_e^2)$ the perpendicular conductivity, and

$$\nu_e = \nu_c + \nu_w + \frac{\alpha_{turb}}{16} \omega_e, \tag{5}$$

where ν_w is the wall-collisionality frequency, and $\alpha_{turb}/16$ is a parameter measuring the relative turbulence level [25]. The other parameters in the equations are typical in the literature.

The integral of eq. 4 along the virtual neutralization surface, Γ_P, provides the backstreaming electron current,

$$I_{e,P} = 2\pi \int_{\Gamma_P} d\chi r j_{e\perp}. \tag{6}$$

The wall-collisionality [1, 2] is related to the secondary electron emission from the wall. The secondary electrons enter into the channel as two unmagnetized beams and produce a 'frictional' effect on the azimuthal drift of the bulk primary electrons. Then, the axial drift has to increase in order to fulfill the momentum conservation

of the electron flow. Although this effect increases the electron current, it is far from satisfying the value that matches the experimental data, and makes the turbulent transport the dominant mechanism in our simulations.

The presence of turbulence, a non-zero effect of phase-correlated azimuthal fluctuations in time, was early observed [6], and was confirmed by the experimental and numerical work of many authors. There is neither a theoretical nor experimental expression for α_{turb}, and normally is tuned to match the experimental discharge current of the thruster I_d, that is the backstreaming electron current, $I_{e,P}$. It has been observed that tailoring appropiately α_{turb}, simulation profiles agree better with experimental ones, but there isn't consensus on the expression for α_{turb}. We assume simply that α_{turb} is constant along the simulation domain. Figure 3 shows the typical values in our simulations of the classical, wall-collisionality, and turbulence frequencies along the thruster.

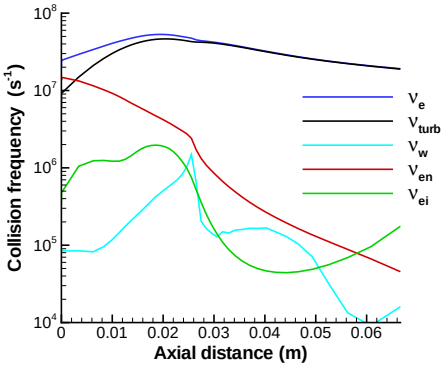

Figure 3. Typical collisional frequencies in our simulations of the SPT-100 Hall thruster.

In this work we focus on the turbulence transport to study the electron current $I_{e,P}$. The numerical experiments and the discussion of results are presented in section 2.3.

2.3. Numerical experiments and discussion

We take the SPT-100 experimental data from ref.[15] to compare and validate our simulation results. The reference simulation parameters of the code are shown in table 1. All the simulation results are averaged along the total simulation time, of the order of $1ms$.

Discharge voltage (V)	300
Anode mass flow rate (mg/s)	5
Maximum radial magnetic field (G)	250
Simulation time step (s)	$5 \cdot 10^{-8}$
Number of particles in simulation	$\sim 10^5$

Table 1. Reference input parameters for plasma simulations.

The first simulation is performed with two goals. First, to compare the experimental data with the numerical ones, and second, to compute the contribution of the double ions in the ion beam current. Table 2 contains the results. The α_{turb} parameter is adjusted to match the experimental discharge current $I_d = 4.5A$.

	α_{turb}	I_d	$I_{e,P}$	$I_{i,P}$	$I_{i,w}$	η
i_1	0.185	4.50	1.48	3.02	1.86	0.334
$i_1 + i_2$	0.165	4.52	1.12	3.40	1.68	0.358

Table 2. Simulation 1 results. Comparison between the reference simulation with only simple ions with the reference simulation with simple and double ions.

The effect of double ions is clear, with a contribution of $\sim 23\%$ in the ion beam current, which increases $\sim 13\%$ from the simple ion simulation. To keep $I_d = 4.5A$ in both simulations, the α_{turb} parameter is reduced about a 10% when double ions are present, which suggests that α_{turb} is an eigenvalue related to the physical parameters of the thruster, but still with a dominant effect on the effective collision frequency ν_e. Moreover, if α_{turb} remains constant in both simulations, $I_{e,P}$ is slightly altered, which reinforces the idea that the electron current is highly dependent on turbulent transport.

The comparison between the experimental and simulated results of table 2 points out two important issues:

- The simulated ion beam current for the simple ions case is lower than the experimental one. The activation of double ions improves the results.
- The turbulent transport is necessary to recover the experimental electron current.

In order to study these two issues, and the relation between them, we have made two numerical experiments:

- The artificial modification of the rate of ionization, with an increase of 10%, 30%, and 50%.
- The variation of α_{turb} in simulations.

In the first case, the simulation 2, we increase homogeneously the ionization rate $\langle R_i \rangle$ of all ionization events in the whole simulation domain, that is, we simply multiplicate the ionization rates by a constant factor f_i. In all cases $\alpha_{turb} = 0.15$ and double ions are activated. The results are shown in table 3.

The ionization is greater, with an increase of a 46% in $\mathcal{I}_{i,tot}$ for the case $f_i = 1.5$. But this larger ionization does not mean more $I_{i,P}$ current, with a slight increment of 7% in the best case. There seems to be a competition between the charge production and the wall losses, who has increased a 106% for $f_i = 1.5$.

In fig.4 we plot the density profiles for different values of f_i. The increase of $I_{i,w}$ is explained by the increase of the

f_i	I_d	$I_{e,P}$	$I_{i,P}$	$I_{i,w}$	$\mathcal{I}_{i,tot}$	η
1.0	4.18	0.85	3.33	1.32	4.79	0.401
1.1	4.40	0.99	3.41	1.66	5.21	0.367
1.3	4.63	1.08	3.55	2.01	5.76	0.400
1.5	4.70	1.14	3.56	2.72	7.00	0.373

Table 3. Simulation 2 results: Variation of the ionization factor f_i. The simulation is performed with reference inputs and double ions activated.

plasma density inside the channel. The energy wall losses increases too as the ionization ratio becomes greater. This fact plus the higher discharge current I_d in the thruster and the higher ionization cost are responsible of the decay in the efficiency of the thruster.

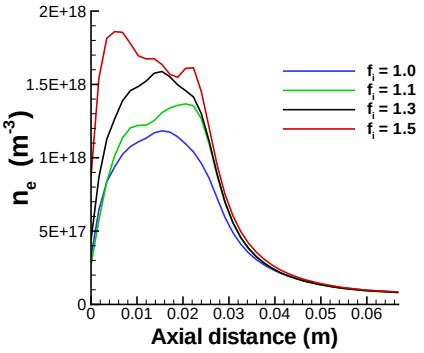

Figure 4. Density profiles of simulation 2.

Simulation 3 is devoted to study the dependence of the electron discharge current with the turbulent transport. The results are shown in table 4.

α_{turb}	I_d	$I_{e,P}$	$I_{i,P}$	$I_{i,w}$	$\mathcal{I}_{i,tot}$	η
0.150	4.18	0.85	3.33	1.32	4.79	0.401
0.160	4.39	1.06	3.33	1.59	5.06	0.356
0.165	4.52	1.12	3.40	1.68	5.19	0.358
0.170	4.57	1.18	3.39	1.70	5.20	0.355

Table 4. Simulation 3 results: variation of the α_{turb} parameter. The simulation is performed with reference inputs and double ions activated.

The discharge current I_d and the ion beam current $I_{i,P}$ are reasonably obtained for $\alpha_{turb} = 0.165$. As expected, the electron current increases as the turbulence parameter is greater, but $I_{i,P}$ remains almost constant. This is because the acceleration region is greater for high values of α_{turb}, see fig. 6, thus the larger ion production observed, $\mathcal{I}_{i,tot}$, is in competition whith the larger ion wall losses, $I_{i,w}$. The increase of $\mathcal{I}_{i,tot}$ obey the larger electron temperature achieved with high values of α_{turb}, fig. 5, and the increase of $I_{i,w}$ is a consequence of the larger plasma density in the channel.

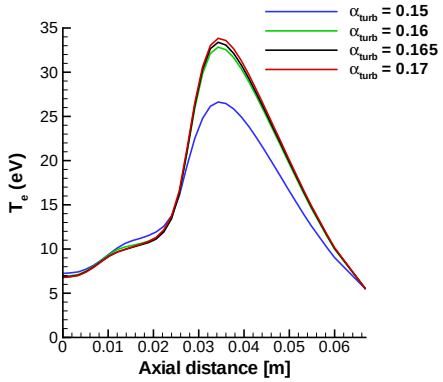

Figure 5. Temperature profiles of simulation 3.

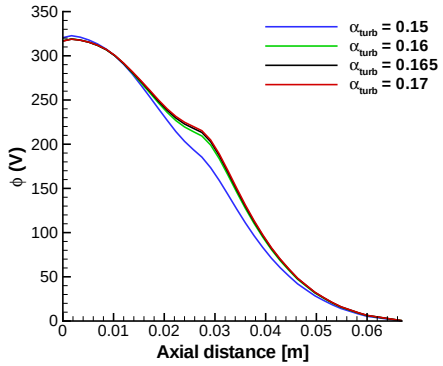

Figure 6. Electric potential profiles for simulation 3.

As a conclusion, we find that the ion beam current does not depend much on the turbulence parameter.

3. PLASMA-WALL INTERACTION

3.1. Fulfillment of the Bohm Condition

The results obtained in the simulations show that the plasma-wall interaction has an important role in the physics of the ion and electron currents. This plasma-wall interaction is dominated by the presence of the sheaths adjacent to the walls. These sheaths are non-neutral boundary layers where the electric potential drops abruptly in order to fulfill the boundary conditions imposed by the walls, that is, zero current for dielectric walls, and a known potential ϕ_W for metallic walls.

It is well known that valid solutions of the electric potential within the sheath are only achieved when the Bohm condition is fulfilled [26]. This condition states that ions must enter into the sheath with a minimum ion velocity, which expression varies depending on the frame theory used: hydrodynamic or kinetic [27].

This issue is important for its numerical implementation

in PIC-based codes of simulation. For that purpose, we have developed an algorithm that weighs correctly the fluxes at the sheaths edges and enforces the kinetic Bohm condition. It is based on the *surface weighting* algorithm [28], with time-filtering techniques and a electric potential adjustment in a thin layer next to the sheath. This adjustment on the potential is small enough to assure a good matching with the sheath solution, but also to reproduce the high non-linearity of the electric field.

Table 5 shows the simulation results using this algorithm in the computations. We observe that $I_{i,w}$ is reduced about a 40%, and $I_{i,P}$ is increased about a 4%, approximately the same increment obtained for an increase of a 50% in the ionization rate. This reduction is mainly explained by the lower plasma density inside the thruster channel, as is shown in fig.7. We conclude that the fulfillment of the Bohm condition has an effect on $I_{i,b}$ more important than the increase of the ionization.

Fulfillment of BC

α_{turb}	I_d	$I_{e,P}$	$I_{i,P}$	$I_{i,w}$	$\mathcal{I}_{i,tot}$	η
0.150	4.25	0.77	3.48	0.87	4.54	0.454
0.160	4.45	0.93	3.52	1.02	4.65	0.438
0.165	4.52	0.99	3.53	1.06	4.70	0.432

No fulfillment of BC

α_{turb}	I_d	$I_{e,P}$	$I_{i,P}$	$I_{i,w}$	$\mathcal{I}_{i,tot}$	η
0.150	4.18	0.85	3.33	1.32	4.79	0.401
0.160	4.39	1.06	3.33	1.59	5.06	0.356
0.165	4.52	1.12	3.40	1.68	5.19	0.358

Table 5. Simulation 4 results: effect of the fulfillment of the Bohm condition. The simulation is performed with reference inputs and double ions activated.

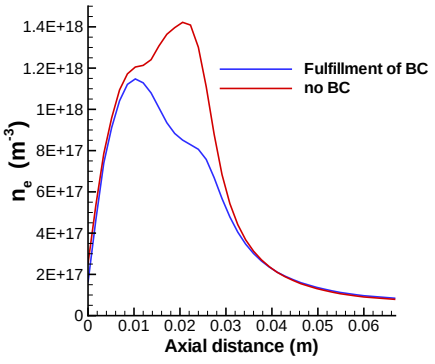

Figure 7. Density profiles for simulation 4.

3.2. Secondary electron emission

Secondary electron emission (SEE) is produced by the interaction of the plasma with the dielectric walls of the thruster. The bulk (or primary) electrons collide with the wall and excite the atomic structure of the ceramic material ($BN-SiO_2$, SiC, Al_2O_3), releasing a new electron that is emitted from the wall, normally at an energy of 1-3 eV. These electrons are the so-called true secondary electrons. The secondary electron emission usually includes primary electrons backscattered at walls.

The SEE yield is determined experimentally, and relates the secondary electron current emited from the wall with the primary electron current. The model we use for the SEE yield in our simulations is

$$\delta_w(T_p) = \left(\frac{T_p}{T_1}\right)^p, \qquad (7)$$

where T_p is the temperature of the confined electron population in the bulk region, T_1 is the crossover temperature for a 100% of SEE yield, which depends on the type of material, and $p \sim 0.5$.

The charge saturation limit makes zero the electric field at the wall, and the total charge within the sheath. In this limit, the effective SEE is maximum and the energy losses are very large.

In order to study the effect of the SEE on the ion and electron currents, we simulated the SPT-100 thruster with different values of T_1 in eq. 7, but maintaining $\alpha_{turb} = 0.15$ in all cases. Table 6 shows the simulation results.

$T_1(eV)$	I_d	$I_{e,P}$	$I_{i,P}$	$I_{i,w}$	$\mathcal{I}_{i,tot}$	η
13.9	3.88	0.56	3.32	0.53	3.98	0.479
26.4	4.18	0.85	3.33	1.32	4.79	0.401
55.5	4.40	1.02	3.38	1.87	5.44	0.369
110.9	4.34	0.99	3.35	2.09	5.70	0.356

Table 6. Simulation 5 results: effect of the secondary electron emission. The simulation is performed with reference inputs and double ions activated.

It is important to observe that $I_{i,P}$ is almost constant and equal to $3.35A$, which means that is not affected by SEE. Once again, there seems to be a certain balance between the gain observed in the ion production $\mathcal{I}_{i,tot}$ and the increase of wall losses. The dependency of $I_{i,wall}$ with the SEE is quite surprising, and is mainly explained by the different density profile observed in figure 8. Lower values of T_1 produce the shift of the ionization region upstream, and the decrease of the plasma density inside the channel, which leads to a lower ion flux reaching the walls. Figure 9 shows the potential profiles for different values of T_1. Moreover, there not seems to be a simple reason for the increase of $I_{e,P}$ with T_1, but the change in the plasma density profile can explain the higher electron conductivity across the B-field.

Figure 10 shows the electron energy flux to the outer wall of the thruster for different values of T_1. The high wall energy losses for low values of T_1 does not explain the increase on the thruster efficiency. A similar result was found by Kim et al.[29]. A priori, it is reasonable to think

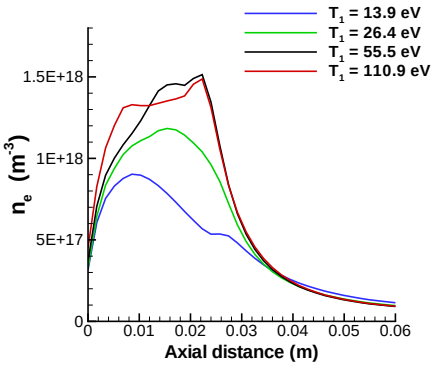

Figure 8. Density profiles for simulation 5.

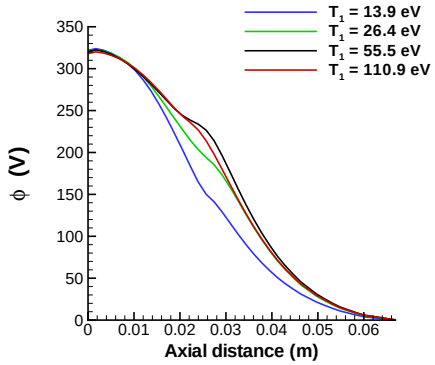

Figure 9. Potential profiles for simulation 5.

that a better performance of the thruster is achieved for high values of T_1. However our simulations show the opposite trend.

We can conclude that the SEE model is an important mechanism to explain and control the electron current in a SPT Hall thruster.

4. IONIZATION BY SECONDARY ELECTRON EMISSION

The ionization observed in simulations is slightly lower than experimental results. We postulate that this difference can be explained by the ionization produced by the SEE.

Secondary electrons, once accelerated by the sheath potential fall, enter as monoenergetic beams into the main plasma where they are magnetized. The dynamics of secondary electrons is determined by the electric field, the magnetic topology, the collisional processes acting upon them, and plasma instabilities.

We concluded in ref.[30] that a trapping effect on the secondary beam is possible for curved and straight oblique

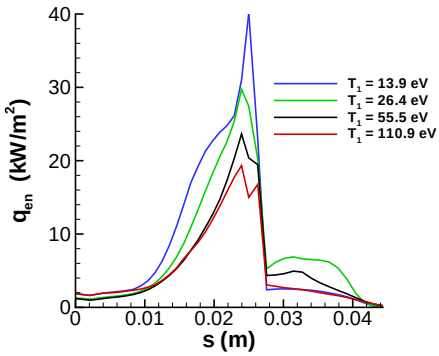

Figure 10. The electron energy flux to the outer wall of the thruster for simulation 5.

magnetic fields, although the determination of the trapped fraction within the bulk of the plasma and the recollected fraction by the walls is hard to predict because of the electron gyromotion.

In this work we assume that secondary electrons are totally thermalized after a typical collision time τ_{col}. The determination of τ_{col} is out of the scope of this paper, and we simply make and educated guess, $\tau_{col} = 10^{-7}s$. Since the sheath-to-sheath flights of the secondary electrons have a typical frequency of $10^8 s^{-1}$, the secondary electrons perform about 10 trips before being thermalized with the primary electron population. Of course this number of trips varies with the angle of the magnetic field at the wall and the sheath potential fall, but 10 seems to be an appropiate order of magnitude.

Along they orbit, secondary electrons conserve the total energy $\mathcal{E}$ and the magnetic moment $\mu = m_e u_\perp^2/2B$ [8]. Since the sheath potential fall ϕ_{sh} is typically several times greater than the energy of emission of the secondary electrons from the wall, the conservation of electron energy within the bulk region reads

$$\mathcal{E} = e\phi_{sh} = \frac{1}{2} m_e u_\parallel^2 + \mu B - e\phi. \qquad (8)$$

In the last expression the mirror effect is included in the μB term.

The recollection of a secondary electron takes place when its kinetic energy perpendicular to the wall, K_w, is greater than the sheath potential barrier $e\phi_{sh}$. This kinetic energy can be estimated at the first trip of the secondary electron's flight. Three typical cases for the phase of gyromotion are:

- a) The velocity vector of the secondary electron has the B-perpendicular component pointing at the wall. In this case K_w is maximum and its expres-

sion is

$$K_w = \frac{1}{2} m_e u_\parallel^2 \cos^2(\alpha_Q) + \mu B \sin^2(\alpha_Q) + 2\sqrt{\frac{1}{2} m_e u_\parallel^2 \mu B \sin^2(2\alpha_Q)}, \quad (9)$$

where $\alpha_Q = \mathbf{B} \cdot \mathbf{N}$ is the magnetic angle at the sheath edge.

- b) The velocity vector of the secondary electron has the B-perpendicular component parallel to the wall. In this case K_w is

$$K_w = \frac{1}{2} m_e u_\parallel^2 \cos^2(\alpha_Q). \quad (10)$$

- c) The velocity vector of the secondary electron has the B-perpendicular component pointing out off the wall. In this case K_w is minimum and its expression depends on the sign of α_Q,

$$K_w = \frac{1}{2} m_e u_\parallel^2 \cos^2(\alpha_Q) \pm \mu B \sin^2(\alpha_Q) \mp 2\sin(2\alpha_Q)\sqrt{\frac{1}{2} m_e u_\parallel^2 \mu B}, \quad (11)$$

where the first case is for $\alpha_Q > 0$ and the second for $\alpha_Q < 0$. Negative values of K_w are a numerical artifact to show that actually the secondary electron does not reach the wall.

Figure 11 shows K_w minus the sheath potential barrier ϕ_{sh} in the three cases for the reference simulation of section 2.3. Secondary electrons are emitted from the inner wall and K_w is computed at the outer wall. Results indicate that the effective confinement of secondary electrons is justified in the regions where $K_w - e\phi_{sh} < 0$, which is almost the whole chamber wall except near the exit region.

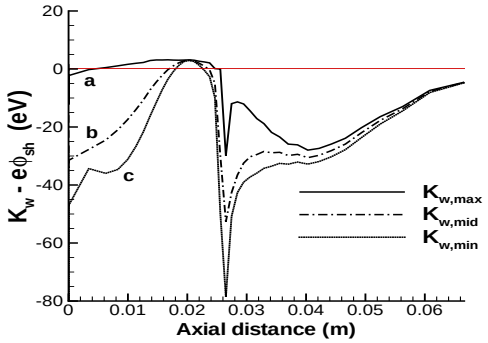

Figure 11. $K_w - e\phi_{sh}$ at the outer wall of the thruster for the three cases of incidence of the secondary electron into the sheath.

Since we are only interested in a first approximation for the ionization produced by SEE, we assume that secondary electron density is constant along the magnetic field lines. This is not really true, but just an estimate.

In our simulations, we adopt the sheath model of Ahedo [16], which takes into account the total thermalization of the secondary beams, and supersonic conditions for ions. The secondary electron density is obtained from the sheath solution, and is related to the sheath potential fall, the SEE yield, and the electron temperature. At the sheath edge, the secondary electron density is

$$\frac{n_s}{n_e} = 1 - \left(1 + \frac{\delta_w \exp\left(\hat{\phi}_{sh}\right)}{1 + erf\left(\sqrt{\hat{\phi}_{sh}}\right)\sqrt{\pi\hat{\phi}_{sh}}}\right)^{-1}, \quad (12)$$

where $\hat{\phi}_{sh} = e\phi_{sh}/T_p$, and the error function is used.

Other sheath models[18] take into account the presence of free secondary electron beams bouncing between the walls, that means the partial thermalization of secondary electrons. Although these sheath models are more consistent with the analysis of the ionization produced by the SEE, we leave that issue for future work.

The ionization rates for secondary electrons are:

$$\begin{aligned} R_{i,0\to1} &= \sigma_{01} v_{sh} \\ R_{i,0\to2} &= \sigma_{02} v_{sh} \\ R_{i,1\to2} &= \sigma_{12} v_{sh} \end{aligned} \quad (13)$$

with $v_{sh} \simeq \sqrt{2e\phi_{sh}/m_e}$, and the σ's are the cross sections for the different ionization events: neutral to simple ion, neutral to double ion, and simple ion to double ion. These cross sections are computed from the experimental cross section models of section 2.1. Figure 12 shows the ionization rates of eq.13.

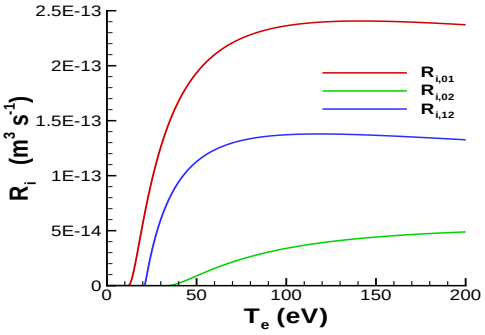

Figure 12. Ionization rates for secondary electrons.

The ion production due to SEE is analogous to eq.1 and 2 updating the new ionization rates of eq.13, and replacing the electron density n_e by the secondary electron density n_s. Is important to note that the lateral wall sheaths are not symmetric, thus the contribution of inner and outer sheaths are different in the total ion production by the secondary electrons.

Figures 13 to 15, show the different ionization fractions $r_i = R_i n_s / \langle R_i \rangle n_e$ caused by secondary electrons. The blank zones in figures represent a ratio lower than a 5%.

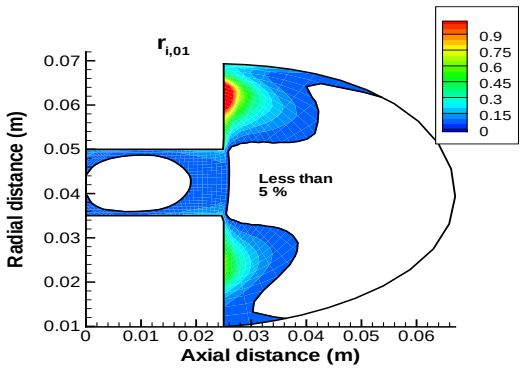

Figure 13. Ratio r_i of the ion production 0-1 by secondary electrons.

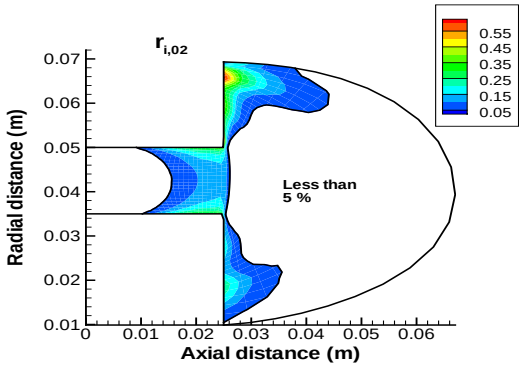

Figure 14. Ratio r_i of the ion production 0-2 by secondary electrons.

Results point out that in the regions (not blanked) of interest of the thruster, the ratio r_i is between $5 - 15\%$. However, this estimation is based on a simple model that does not take into account the charge conservation equation of the secondary electrons along the magnetic field lines.

5. CONCLUSIONS

The understanding on the Hall discharge and the generation of a reliable simulation code require the analysis of the physical processes that govern and affect the ion beam current and the electron backstreaming current inside the thruster. These physical processes compose a complex interplay of phenomena in the Hall discharge. The ion production and the ion wall losses represent the key factors to understand the ion beam current, whereas the turbulent difussion is the main mechanism to understand the electron current. Both currents are much affected by the plasma-wall interaction, either by the secondary electron emission or by numerical issues concerning the fulfillment of the bohm condition. In this work a question has raised regarding the benefits obtained on thrust efficiency caused by higher secondary electron emission, which is at

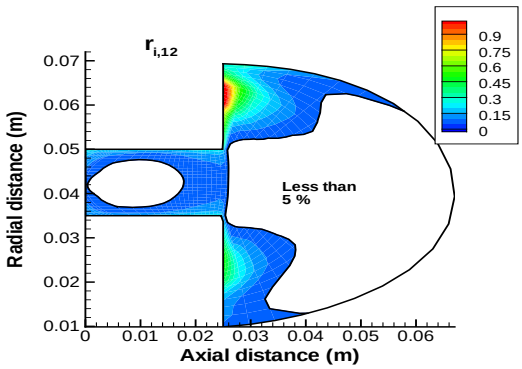

Figure 15. Ratio r_i of the ion production 1-2 by secondary electrons.

odds with common opinion, but agrees with some experimental results. Finally, the estimation of the ionization produced by the secondary electrons has been studied in order to explain the difference between the ionization results of simulations and the experimental ones. However, our estimation does not let us to reach a clear conclusion on that matter.

ACKNOWLEDGMENTS

This research was financed by the Ministerio de Ciencia e Innovación of Spain, under project ESP-20007-62694.

REFERENCES

[1] A. I. Morozov, Y. V. Esipchuk, G. N. Tilinin, A. V. Trofimov, Y. A. Sharov, and G. Y. Shchepkin. Sov. Phys. Tech. Phys., vol 17, no. 1, pp. 38-45, Jul. 1972.

[2] E. Ahedo. Physics of plasmas 9, 4340(2002).

[3] E. Ahedo, J. M. Gallardo, M. Martínez-Sánchez. Physics of plasmas 10, 3397(2003).

[4] F. Parra, E. Ahedo, M. Fife, and M. Martínez-Sánchez. Journal of Applied Physics **100**, 023304 (2006).

[5] L. Garrigues, G. J. M. Hagelaar, C. Boniface, and J. P. Boeuf. Journal of Applied Physics **100**, 123301 (2006).

[6] G. S. Janes, R. S. Lowder. Physics of fluids 9, 1115 (1966).

[7] J. C. Adam, A. Herón, and G. Laval. Physics of plasmas **11**, no.1, pp. 295-305 (2004).

[8] J. A. Bittencourt. *Fundamentals of plasma physics.* Pergamon Press.

[9] J. W. Koo and I. D. Boyd. Physics of plasmas **13**, no.3, pp. 033501-1-033501-7 (2006).

[10] G. J. M. Hagelaar and J. Bareilles and L. Garrigues and J.P. Boeuf. Journal of Applied Physics 93, 67 (2003).

[11] R.R. Hofer, I. G. Mikellides, I. Katz, and D. M. Goebel. Proceedings of 43rd Joint propulsion conference and exhibit, AIAA 2007-5267 (2007).

[12] M. K. Scharfe, N. Gascon, M. A. Cappelli, and E. Fernandez. Physics of plasmas **13**, no.8, pp. 083505-1-083505-12 (2006).

[13] J. Fox, A. A. Batischeva, O. V. Batischev, and M. Martinez-Sanchez. Proceedings of 42th Joint propulsion conference and exhibit, AIAA 2006-4324 (2006).

[14] I. Katz, R. Hofer, and D. M. Goebel. IEEE Transactions on plasma science **36**, no.5, October 2008.

[15] J. M. Sanlovic, J. A. Hamley, and T. W. Haag. Proceedings of International Electric Propulsion Conference, IEPC-93-094 (1993).

[16] D. Escobar and E. Ahedo, IEEE Transactions on Plasma Science **36**, 2043 (2008).

[17] F. Parra, D. Escobar, and E. Ahedo. Proceedings of 42nd Joint propulsion conference and exhibit, AIAA 2006-4830 (2006).

[18] I. Maqueda, D. Escobar, and E. Ahedo. IEPC 2007-066, Electric Rocket Propulsion Society, Fairview Park, OH, 2007.

[19] A. Bishaev and V. Kim. Sov. Phys. Tech. Phys. **23**, 1055 (1978).

[20] E. Ahedo, P. Martínez-Cerezo, M. Martínez-Sánchez. Physics of plasmas 8, 3058 (2001).

[21] E. Ahedo, D. Escobar. Journal of applied physics 96, 983 (2004).

[22] M. Mitchner and C. K. Krueger. *Partially Ionized Gases.* John Wiley & Sons, New York (1973).

[23] D. Mathur and C. Badrinathan. Physical Review A 35, 1033 (1987).

[24] E. W. Bell, N. Djuric, and G. H. Dunn. Physical Review A, vol. **48**, no.6, Dec 1993.

[25] E. Ahedo, J. M. Gallardo, M. Martínez-Sánchez. Physics of plasmas 9, 4061(2002).

[26] K. U. Riemann. IEEE Transactions on plasma science, vol.**23**, no.4, Aug. 1995.

[27] E.R. Harrison, and W. B. Thompson. Proc. Phys. Soc. 74 145, 1959.

[28] D. Escobar, E. Ahedo, and F.I. Parra. IEPC 2005-041, Electric Rocket Propulsion Society, Princeton university, NJ, 2005.

[29] V. Kim, V. kozlov, A. Skrylnikov, A. Veselovzorov, N. Hilleret, B. Henrist, S. Locke, and J. M. Fife. Proceedings of 39th Joint propulsion conference and exhibit, AIAA 2003-5002 (2003).

[30] R. Santos, and E. Ahedo. Proceedings of 44th Joint propulsion conference and exhibit, AIAA 2008-4725 (2008).

[31] V. V. Zhurin, H. R. Kaufman, R. S. Robinson. Plama sources Sci. Technology 8, R1-R20 (1999).

[32] S. Yoshikawa, D. J. Rose. Physics of fluids 5, 334 (1962).

[33] A. I. Morozov and V. V. Savelyev. Proceedings of International Electric Propulsion Conference (1995).

[34] A. I. Bugrova and A. I. Morozov and V. K. Kharchevnikov. Sov. Phys. Tech. Phys. 30, 610 (1985).

[35] V. Kim. J. Propul. Power **14**, 736 (1998).